Analysis of Mojette Transform Projections using Z3 lattice versus A3 lattice

Vincent Ricordel, Nicolas Normand, Jeanpierre Guédon

Analysis of Mojette Transform Projections using Z^3 lattice versus A^3 lattice

Vincent Ricordel Nicolas Normand
Jeanpierre Guédon *
{vincent.ricordel; nicolas.normand; jeanpierre.guedon}@univ-nantes.fr

Université de Nantes, LS2N UMR CNRS 6004
Polytech Nantes, rue Christian Pauc BP 50609, 44306 Nantes Cedex 3, France

Abstract

The Mojette Transform (MT) is an exact discrete form of the Radon transform. It has been originally defined on the cubic lattice Z^n (where n is the dimension). We propose to study this transform when using the densest lattice for the dimension 3, namely the face-centered cubic lattice A^3. In order to compare the legacy MT using Z^3, versus the new MT using A^3, we use a fair comparison methodology between the two MT schemes. Statistic criteria have been defined to analyse the information distribution on the projections. The experimental results show the specific nature of the information distribution on the MT projections due to the compacity of the A^3 lattice.
Keywords Mojette Transform, Discrete Tomography, Lattices, Densest Lattices.

1 Objectives of the study

The Mojette transform is an exact discrete form of the Radon transformdefined for specific rational projection angles. Guédon *et al.* originally developed this transform and its corresponding inverse in 1995, in order to represent an image as a set of discrete projections which can be chosen highly redundant. Since, the MT properties have been largely explored and a lot of applications have been found [1]. The MT has been mainly defined, studied and applied using the cubic lattice Z^n (where n is the dimension of the initial grid to transform). We propose to study this transform when using densest lattices, because we expect that the lattice high compacity will improve the MT performances when representing the data. In the paper we focus the study by considering the dimension 3.
The paper is organised as follows: in the second section, basics on MT and lattices are given. Exactly, we present the MT properties that are used in the paper, and the densest lattice for the dimension 3 namely the face-centered cubic lattice A^3. In the third section, a fair comparison method between the two MT schemes is defined. The fourth section explains the statistic criteria used to analyse the information distribution on the MT projections, and gives the experimental results. A conclusion is given in the last section.

*Thank to Ugo Maury and Maxime Pineau who worked on this project for their MSc at Polytech Nantes.

2 Basics on Mojette Transform and Lattices

2.1 The Mojette Transform

2.1.1 Direct Transform

The Mojette transform is an exact discrete form of the Radon transform defined for specific rational projection angles [2]. These angles θ_i are defined by a set of discrete vectors (p_i, q_i) as $\theta_i = \tan(q_i, p_i)$, with the condition that q_i and p_i are coprime (i.e. $\gcd(p_i, q_i) = 1$), and q_i is restricted to be positive except for the case $\{p_i, q_i\} = (1, 0)$. The transform domain of an image (or any 2D grid) is a set of

projections where each element (called bin) corresponds to the sum of the pixels centered on the line of projection. This is a linear transform defined for each projection angle by the operator:

$$[\mathcal{M}f](b,p,q) = proj_{p,q}(b) = \sum_{k=-\infty}^{\infty}\sum_{l=-\infty}^{\infty} f(k,l).\Delta(b+kq-lp) \quad (1)$$

where (k,l) defines the location of an image pixel, b is the bin index, and $\Delta(n)$ is the Kronecker delta function. Equation (1) can be rewritten in a matrix form:

$$[\mathcal{M}f](b,p,q) = \sum_{k}\sum_{l} f(k,l).\Delta\left(\mathcal{B} - \mathcal{P}_{2\to1}\begin{bmatrix}k\\l\end{bmatrix}\right) \quad (2)$$

where $\mathcal{B} = b$, and $\mathcal{P}_{2\to1}\begin{bmatrix}k\\l\end{bmatrix}$ is the projection matrix.

Equation (2) can be generalised to higher dimensions. In 3D, a projection plane is defined by a discrete vector (p,q,r) with $gcd(p,q,r) = 1$. In the same way, the projection planes are built from a discrete 3D volume $f(k,l,m)$. Bins are discrete points onto the projected plane, indexed by a vector $\mathcal{B} = \begin{bmatrix}b_1 & b_2\end{bmatrix}^t$. The 3D Mojette transform is then defined as [3], [4]:

$$\mathcal{M}f(b_1,b_2,p,q,r) = \sum_{k,l,m} f(k,l,m).\Delta\left(\mathcal{B} - \mathcal{P}_{3\to2}\begin{bmatrix}k\\l\\m\end{bmatrix}\right) \quad (3)$$

In order to obtain a simple and unique index method for the vector of projection, the following conventions are taken [3]: $r \geq 0$ and $q \geq 0$ if $r = 0$. The projection $\mathcal{P}_{3\to2}$ matrix has been first defined in[3]. Its computation has been optimised in order to ensure entire displacements and points with integer coordinates [5], [6]. So the projection of a 3D regular grid on a plane with the vector (p,q,r) always produces a 2D regular grid[4].

2.1.2 Projection matrix and reconstructibility

The reconstructability is the ability to ensure the exact reconstruction of any information using only a set of viewpoints. In other words, an region is reconstructible by a set of projections if a unique correspondence exists between the region and the set of projections [7]. The reconstructability conditions depends strongly on the discrete shape of the region support under projection. Simple rules exist for 2D convex shapes[2], [8]. The reconstruction conditions for any convex region were derived by Normand [8].

In 2D, each projection direction vector (p_i,q_i) is associated with a two-pixels structuring element B_i (2PSE). Taking G as the region support formed by the successive dilations of the structuring elements B_i, the convex region is reconstructible if and only if it can not contain G [7], [8]. The method is directly extended [4] in 3D: each projection direction vector (p_i,q_i,r_i) is associated with a two-voxels structuring element, and any convex 3D region R is reconstructible by a set of projections, if the dilation of the two-voxels structuring elements produces a form than is not included in R.

2.2 The lattices

2.2.1 Lattices

A lattice Λ is a regular arrangement of points in a n-dimensional space. Λ is characterised by its basis [9] or correspondingly by its *generator matrix* M. By combination of the basis vectors, the lattice *fundamental parallelotope* is constructed. This parallelotope, when repeated, can fill the whole space with just one lattice point in each copy.

Different lattices have been studied to solve different problems as sphere packing problem, sphere covering problem, kissing number, fast quantisation, *etc.* In the paper we focus on the dimension $n = 3$, with the cubic lattice Z^3, and on the densest lattice for this dimension, namely A^3.

A sphere packing is an arrangement of non-overlapping identical spheres within a containing space. The lattice is then constituted with the spheres centers, and the densest packing maximises the volume occupied by the spheres. The lattice density can be defined by:

$$\Delta = \frac{\text{vol. of one sphere}}{\text{vol. of the fundamental region}} = \frac{\text{vol. of one sphere}}{det(MM^{tr})^{\frac{1}{2}}} \quad (4)$$

2.2.2 Z^n lattices

The cubic lattice, also known as the integer lattice, is defined as [9]:

$$Z^n = \{(x_1, \ldots, x_n) | x_i \in \mathbb{Z}\} \tag{5}$$

Its generator matrix is the identity matrix. The density of the lattice Z^3 is $\Delta_{Z^3} = \frac{\pi}{6} = 0.524...$

We will exploit the lattice symmetries for the MT. The Z^n automorphism group consists of all possible symmetries that are obtained by vector coordinates permutation and/or sign change, it is equal to $(2^n * n!)$. So, after removing the sign changes, Z^3 counts 24 symmetries (see figure 1).

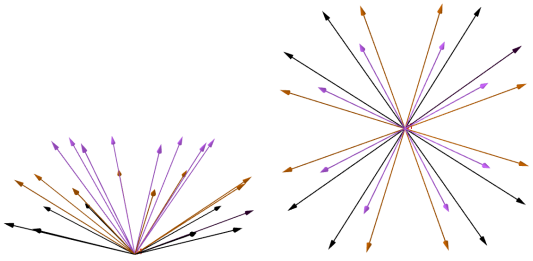

(a) Side view. (b) Top view.

Figure 1: Symmetry in Z^3 (without sign change).

2.2.3 A^n lattices

The A^n lattice (for $n \geq 1$) can be defined as:

$$A^n = \{(x_0, \ldots, x_n) \in Z^{n+1} | x_0 + x_1 + \cdots + x_n = 0\} \tag{6}$$

Its generator matrix is [9] :

$$M_{A^n} = \begin{bmatrix} -1 & 1 & 0 & 0 & \ldots & 0 & 0 \\ 0 & -1 & 1 & 0 & \ldots & 0 & 0 \\ 0 & 0 & -1 & 1 & \ldots & 0 & 0 \\ \vdots & \vdots & \vdots & \vdots & \ddots & \vdots & \vdots \\ 0 & 0 & 0 & 0 & \ldots & -1 & 1 \end{bmatrix} \tag{7}$$

A^n is the densest lattice for the dimension 3. A^3 is also known as the face-centered cubic lattice (FCC), its density is $\Delta_{A^3} = \frac{\pi}{\sqrt{18}} = 0.7405....$ The automorphism group of the lattice A^3 equals 48, after removing the sign changes, 12 symmetries are remaining [9] (see also the figure 2).

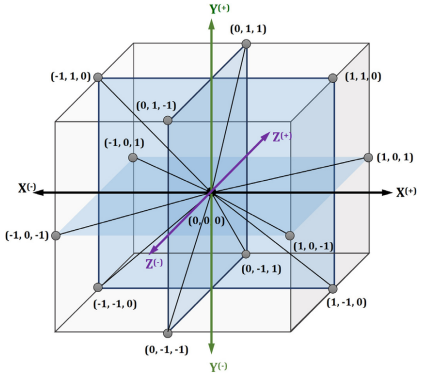

Figure 2: Neighbors of the point $(0, 0, 0)$ in A^3 [10]

2.3 Projections and Haros-Farey sequences

The Haros-Farey sequence gives the set of rational angles in a centered square or cube, this sequence is used to enumerate the MT projections (up to the reconstructability conditions).

In 3D, according to [6], the Haros-Farey sequence of order N, noted $\widehat{F}_N$, is the set of points $(\frac{y}{x}, \frac{z}{x})$ such as $gcd(x, y, z) = 1$, between $[0, 0]$ and $[1, 1]$, and which denominator x does not exceed N. In other words, a point $(\frac{y}{x}, \frac{z}{x}) \in \widehat{F}_N$ if $x \leq N$, $0 \leq y \leq x$, $0 \leq z \leq x$ and if $gcd(x, y, z) = 1$. Let $A_1(\frac{y_1}{x_1}, \frac{z_1}{x_1})$ and $A_2(\frac{y_2}{x_2}, \frac{z_2}{x_2})$, two points of $\widehat{F}_{N-1}$ such as $x_1 + x_2 = N$. The median point between A_1 and A_2 has the coordinates $(\frac{y_1+y_2}{x_1+x_2}, \frac{z_1+z_2}{x_1+x_2})$ [6]. The sequence is used in order to generate the (p, q, r) projections of the 3D MT, with (p, q, r) representing the point $(\frac{q}{p}, \frac{r}{p})$.

3 Comparison

The section explains how the 3D grids were constructed and how the projections were selected. The proposed criteria of comparison are also presented.

3.1 Methodology of comparison

3.1.1 Grids construction

The goal is to compare the legacy MT using the Z^3 grid, with the MT using the densest grid A^3. Each grid (Z^3 or A^3) is truncated such as it counts the

same number of points N_{points}. An iterative process is used where, from the 0 point, at each loop, we find the lattice points on successive embedded spheres. Locally, a basic pattern is used which gives for a lattice point its closed neighbours (see figures 1 and 2). The growing lattice process is stoped when the number of points N_{points} is reached. Each point of the grids is set to an unitary value.

3.1.2 Selection of projections

Just enough projections are chosen for the grid to be exactly reconstructible. Projection vectors are produced by sorting fractions of Haros-Farey series according to their squared Euclidean norms, *i.e.*, respectively $x^2+y^2+z^2$ and $xx+yy+zz-yz-xz$, in lattices Z^3 and A^3.

Before choosing another projection in the Haros-Farey set, all equivalent projections by rotation are generated. The number of equivalent projection by rotation depends on the lattice symmetries.

In order to know if the grid is exactly reconstructible using the set of selected projections, the shape of successive dilatations of the projections directions is generated, as explained in section 2.1.2. The grid is exactly reconstructible only when its radius is inferior or equal to the radius of the generated figure [12].

3.2 Comparison criteria

Global criteria were used to compare the information distribution on the MT projections.

3.2.1 The Redundancy

The redundancy is given by [3]:

$$Red = \frac{nb_{bins}}{nb_{pixels}} - 1 \tag{8}$$

If the redundancy is positive, it represents the percentage of extra bins compare to the number of points. If the redundancy is negative, then there is no reconstructability of the grid.

3.2.2 The bins number, mean and variance

B_i is the bins number on the i-th projection (i.e. the i-th projection length). The bins number mean B_m and the bins number variance B_v can be then calculated as following [11], [12]:

$$B_m = \frac{1}{n}\sum_{i=1}^{n} B_i, \quad B_v = \frac{1}{n}\sum_{i=1}^{n}(B_i - B_m)^2 \tag{9}$$

where n is the number of projections in the set. This criteria measures the difference of bins number in the projections. The smaller B_v for different projections, the higher those projections carry the same amount of information [12].

3.2.3 The points number mean per bin

For the test case, each grid point is set to 1, so each bin value (on every projections) equals to the number of points that contribute to the bin. The points number mean per bin for all bins (in all projections) is computed as [12]:

$$Mean(\text{points per bin}) = b_m = \frac{1}{m}\sum_{i=1}^{m} b_i \tag{10}$$

where m is the total number of bins (considering all projections) and b_i is the value of the i-th bin. The higher the mean, the higher bins represent more points. This is directly related to the density of the lattice.

4 Experimental results

In this section, the main results are presented and discussed. On each figure, the blue (resp. red) curve characterises the A^3 (resp. Z^3) lattice. The first feature displayed on figure 3(a) is the grid radius value computed from N_{points}, the number of generated points. For $N_{points} > 400$, the curves show the higher compacity of A^3 on Z^3.

The higher total number of bins of Z^3 (see figure 3(b)) explains its higher redundancy (see figure 3(c)).

The next features are the number of bins Mean (figure 4(a)) and Variance (figure 4(b)) according to the number of generated points. Concerning these 2 features, it seems that the two grids performs almost equally, but the figure 4(c) shows that the projections number is different for the 2 lattices, a finer analysis at the projections level is then necessary.

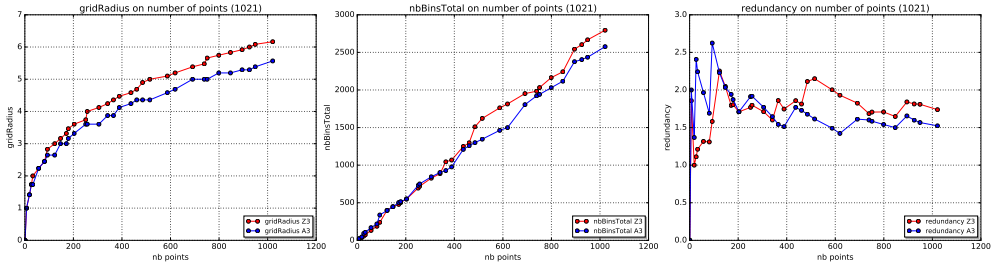

(a) (b) (c)

Figure 3: Grid radius (a), Total number of bins (b), and Redundancy (c). The blue (resp. red) curves characterise the A^3 (resp. Z^3) lattice.

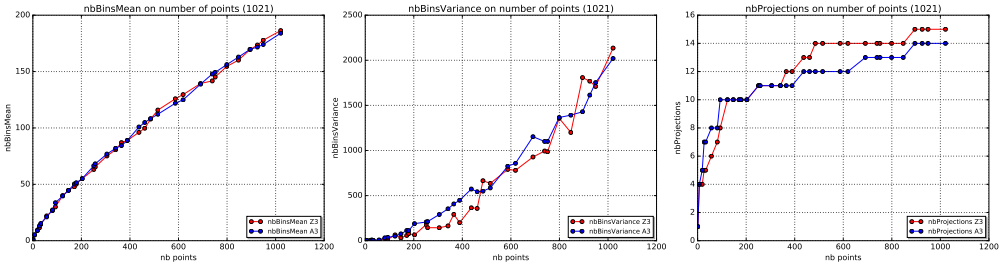

(a) (b) (c)

Figure 4: Number of bins Mean (a) and Variance (b), and redundancy (c). The blue (resp. red) curves characterise the A^3 (resp. Z^3) lattice.

We then use histograms. The figure 5 compares the projections densities considering the number of points mean per projection. And the figure 6 compares the projections densities considering their lengths. The histograms with A^3 are slightly smoother that the ones with Z^3, it shows the higher regularity of the projections when using A^3, these results are due to the high compacity of this lattice.

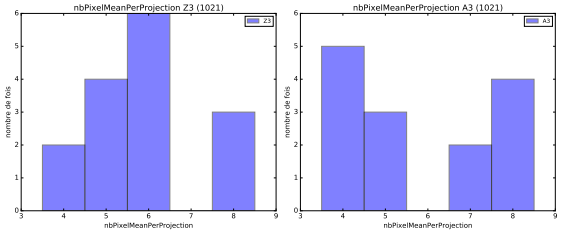

(a) (b)

Figure 5: Histograms of the number of points mean per projection for Z^3 (a) and A^3 (b).

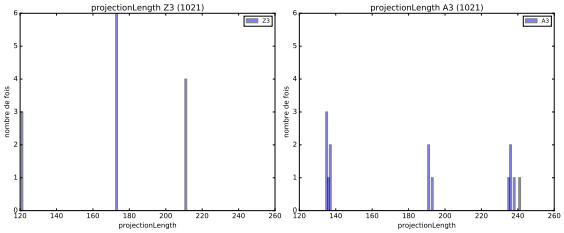

(a) (b)

Figure 6: Histograms of the projections length for Z^3 (a) and A^3 (b).

5 Conclusion & perspectives

In this paper, we examined the behaviour of the densest lattice in 3D from its discrete Mojette projections point of view. The analysis of Mojette Transform projections, when comparing the legacy

MT with Z^3 versus the MT with A^3, shows some interesting differences in terms of dimensions, and in terms of projections regularity. Since the software has been developed to manage any dimensions and lattices, the next work will focus on higher dimensions. Indeed it seems interesting to try higher dimensions in order to see if the gap between A^n and Z^n lattices still increases.

References

[1] J. Guédon, *The mojette transform: Theory and applications*. Wiley-ISTE, 2009, ISBN: 978-1-84821-080-6. [Online]. Available: https://hal.archives-ouvertes.fr/hal-00367681.

[2] M. B. Katz, "Questions of uniqueness and resolution in reconstruction from projections", in *Lecture Notes in Biomath*, vol. 26, 1978.

[3] J.-P. Guédon and N. Normand, "Direct mojette transform", in *The Mojette Transform: Theory and Applications*, Wiley-ISTE, 2009, ch. 3, pp. 41–66, ISBN: 978-1-84821-080-6. [Online]. Available: https://hal.archives-ouvertes.fr/hal-00367681.

[4] J. Guédon, N. Normand, and S. Lecoq, "Transformation mojette en 3d : Mise en oeuvre et application en synthèses d'images", Sep. 1999. [Online]. Available: http://hdl.handle.net/2042/13101.

[5] N. Normand, M. Servières, and J. Guédon, "How to obtain a lattice basis from a discrete projected space", in *Discrete Geometry for Computer Imagery 2005*, É. Andres, G. Damiand, and P. Lienhardt, Eds., ser. Lecture Notes in Computer Science, vol. 3429, Poitiers, France: Springer Berlin / Heidelberg, Apr. 2005, pp. 153–160, ISBN: 978-3-540-25513-0. DOI: 10.1007/978-3-540-31965-8_15.

[6] M. Servières, "Reconstruction Tomographique Mojette", Theses, Université de Nantes ; Ecole Centrale de Nantes (ECN), Dec. 2005. [Online]. Available: https://tel.archives-ouvertes.fr/tel-00426920.

[7] N. Normand and J.-P. Guédon, "La transformée mojette: Une représentation redondante pour l'image", *Comptes Rendus de l'Académie des Sciences - Series I - Mathematics*, vol. 326, no. 1, pp. 123–126, 1998, ISSN: 0764-4442. DOI: http://dx.doi.org/10.1016/S0764-4442(97)82724-3.

[8] J.-P. Guédon and N. Normand, "Reconstructability with the inverse mojette transform", in *The Mojette Transform: Theory and Applications*, Wiley-ISTE, 2009, ch. 4, pp. 67–84, ISBN: 978-1-84821-080-6. [Online]. Available: https://hal.archives-ouvertes.fr/hal-00367681.

[9] J. H. Conway and N. J. A. Sloane, *Sphere packings, lattices and groups*, ser. Grundlehren der math. Wissenschaften. Springer, 1993, vol. 290.

[10] M. A. Rashid, S. Iqbal, F. Khatib, M. T. Hoque, and A. Sattar, "Guided macromutation in a graded energy based genetic algorithm for protein structure prediction", *Computational biology and chemistry*, vol. 61, pp. 162–177, 2016. DOI: 10.1016/j.compbiolchem.2016.01.008.

[11] V. Ricordel, "Mojette transform: Square vs. hexagonal lattices", in *Mojette Day*, Apr. 2016.

[12] C. Rougale and J. Thomas, "The Mojette transform on regular non-cubic grids", 2015.

[13] É. Andres, G. Damiand, and P. Lienhardt, Eds., *Discrete geometry for computer imagery 2005*, vol. 3429, ser. Lecture Notes in Computer Science, Poitiers, France: Springer Berlin / Heidelberg, Apr. 2005, ISBN: 978-3-540-25513-0. DOI: 10.1007/b135490.